AGU PUBLICATIONS

Tectonics

RESEARCH ARTICLE
10.1002/2015TC003968

Key Points:
- The shrinking-plate hypothesis predicts subtle differences in azimuths of right-lateral versus left-lateral transform faults
- Transform-fault azimuths observed globally indicate a statistically significant difference between right-lateral and left-lateral faults
- Transform faults do not precisely parallel plate motion, thus validating inferred quantifiable plate nonrigidity

Supporting Information:
- Supporting Information S1

Correspondence to:
R. G. Gordon,
rgg@rice.edu

Citation:
Mishra, J. K., and R. G. Gordon (2016), The rigid-plate and shrinking-plate hypotheses: Implications for the azimuths of transform faults, *Tectonics*, *35*, 1827–1842, doi:10.1002/2015TC003968.

Received 14 JUL 2015
Accepted 10 MAY 2016
Accepted article online 23 MAY 2016
Published online 12 AUG 2016

©2016. American Geophysical Union. All Rights Reserved.

The rigid-plate and shrinking-plate hypotheses: Implications for the azimuths of transform faults

Jay Kumar Mishra[1] and Richard G. Gordon[1]

[1]Department of Earth Science, Rice University, Houston, Texas, USA

Abstract The rigid-plate hypothesis implies that oceanic lithosphere does not contract horizontally as it cools (hereinafter "rigid plate"). An alternative hypothesis, that vertically averaged tensional thermal stress in the competent lithosphere is fully relieved by horizontal thermal contraction (hereinafter "shrinking plate"), predicts subtly different azimuths for transform faults. The size of the predicted difference is as large as 2.44° with a mean and median of 0.46° and 0.31°, respectively, and changes sign between right-lateral (RL)-slipping and left-lateral (LL)-slipping faults. For the MORVEL transform-fault data set, all six plate pairs with both RL- and LL-slipping faults differ in the predicted sense, with the observed difference averaging 1.4° ± 0.9° (95% confidence limits), which is consistent with the predicted difference of 0.9°. The sum-squared normalized misfit, *r*, to global transform-fault azimuths is minimized for $\gamma = 0.8 \pm 0.4$ (95% confidence limits), where γ is the fractional multiple of the predicted difference in azimuth between the shrinking-plate ($\gamma = 1$) and rigid-plate ($\gamma = 0$) hypotheses. Thus, observed transform azimuths differ significantly between RL-slipping and LL-slipping faults, which is inconsistent with the rigid-plate hypothesis but consistent with the shrinking-plate hypothesis, which indicates horizontal shrinking rates of 2% Ma^{-1} for newly created lithosphere, 1% Ma^{-1} for 0.1 Ma old lithosphere, 0.2% Ma^{-1} for 1 Ma old lithosphere, and 0.02% Ma^{-1} for 10 Ma old lithosphere, which are orders of magnitude higher than the mean intraplate seismic strain rate of ~10^{-6} Ma^{-1} (5×10^{-19} s^{-1}).

1. Introduction

The central tenet of plate tectonics, which has revolutionized our understanding of how our planet works, is that the plates are rigid. In contrast, *Kumar and Gordon* [2009] argued that tectonic plates are not rigid but instead shrink horizontally due to thermal contraction as oceanic lithosphere cools [*Collette*, 1974]. The shrinking is most rapid for newly created lithosphere and decreases as $\approx t^{-1}$ where *t* is age [*Kumar and Gordon*, 2009]. Predicted shrinking of the Pacific plate indicates intraplate displacement rates of up to ≈2 mm a^{-1} [*Kreemer and Gordon*, 2014].

Several lines of evidence indicate that the lithosphere fully contracts horizontally in response to thermal contractional stress averaged vertically from the top of the lithosphere to the brittle-plastic transition, taken to be an isotherm below which differential stress is relaxed over geologic time by creeping flow [*Turcotte and Oxburgh*, 1967, 1969; *Kohlstedt et al*., 1995]. First, the observed variation of depth with age agrees well with thermal models that predict the depth of oceanic lithosphere while assuming that thermal contraction occurs horizontally as well as vertically [*McKenzie*, 1967; *Parsons and Sclater*, 1977; *Smith and Sandwell*, 1997; *Hillier and Watts*, 2005]. Second, earthquake focal mechanisms indicate that the upper part of the seismogenic oceanic lithosphere is generally in horizontal deviatoric compression and that the lower part is in horizontal deviatoric tension [*Wiens and Stein*, 1984; *Bergman et al*., 1984; *Huang et al*., 2015]. Models of thermoelastic stresses in cooling oceanic lithosphere predict this observed state of stress if the lithosphere is assumed to contract freely to relieve the vertically averaged thermal stresses [*Sandwell*, 1986; *Haxby and Parmentier*, 1988; *Wessel and Haxby*, 1990; *Wessel*, 1992]. Third, the geoid anomaly observed across fracture zones also has been successfully predicted by incorporating the effects of flexure due to thermal bending stresses if the lithosphere is assumed to contract freely to relieve the vertically averaged thermal stresses [*Parmentier and Haxby*, 1986]. Fourth, formation of gravity lineaments has been attributed to thermal contraction and corresponding models have been shown to match the observed gravity amplitudes and crack spacings if the lithosphere is assumed to contract freely to relieve the vertically averaged thermal stresses [*Sandwell and Fialko*, 2004].

In contrast, *Korenaga* [2007] disputes these multiple lines of evidence and postulates that thermal stresses are relieved by the formation of deep vertical cracks in the lithosphere.

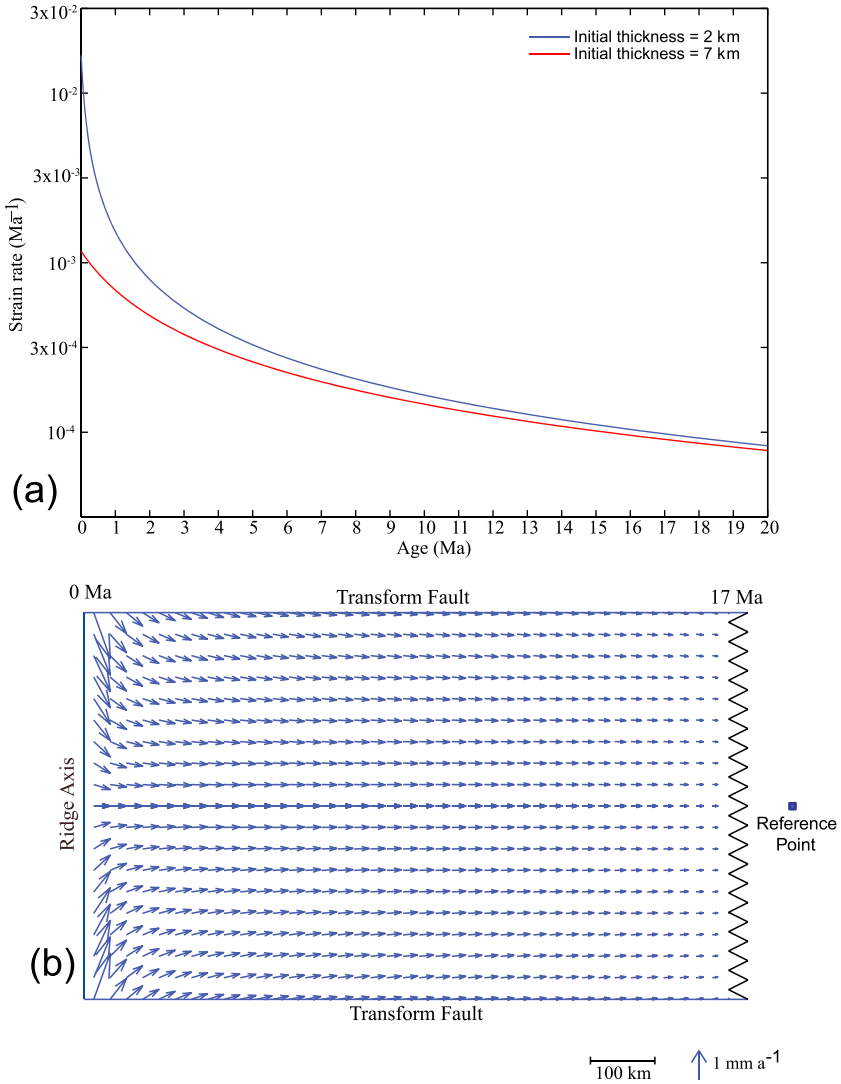

Figure 1. (a) Strain rate of horizontal thermal contraction (assuming free contraction) versus age for two different values of zero-age thickness of the lithosphere. A 2 km thickness (blue curve) is appropriate for fast spreading and is used in the calculations herein. A 7 km thickness (red curve) is appropriate for ultraslow spreading and gives lower rates of contraction for very young lithosphere. (b) Horizontal displacement rates due to horizontal thermal contraction of a rectangular segment of lithosphere relative to a reference point, arbitrarily chosen to be located at a distance of 1500 km from the ridge, in the old interior of the plate along the median line perpendicular to the ridge. Ridge segment length is 600 km, transform offset length is 1000 km, and spreading half rate is 60 mm a^{-1}. Velocities are in a reference frame in which the reference point is held fixed and the median line does not rotate.

Herein we explore the possible effect of horizontal thermal contraction on the azimuths of transform faults with the aim of using an additional set of observations to distinguish between the rigid-plate hypothesis and the shrinking-plate hypothesis. *Roest et al.* [1984] previously examined the hypothesis that the spacing between fracture zones change with age due to thermal contraction acting in concert with other tectonic forces in the central Atlantic. Our approach differs in that we focus entirely on the zone of active strike-slip faulting in transform faults and that we analyze global data.

Age-dependent transform-fault-perpendicular and transform-fault-parallel displacement rates are first obtained from *Kumar and Gordon*'s [2009] formulation for cumulative displacement rate with age for oceanic lithosphere assuming orthogonal spreading (Figure 1). Predicted biases in transform-fault azimuths are then determined from the predicted transform-fault-perpendicular displacement rates. Here we take the bias to be the azimuth predicted for a shrinking plate minus the azimuth predicted for a rigid plate

(i.e., the direction of relative plate motion). We apply the predicted bias to 139 observed transform-fault azimuths distributed between 15 plate pairs modified slightly from the MORVEL transform-fault data set [*DeMets et al*., 2010]. Thus, we test whether a significantly better fit to the data is obtained after correction for the predicted bias.

We find that the predicted bias in transform-fault azimuths caused by horizontal thermal contraction varies in magnitude between 0.01° and 2.44° with a mean value of 0.46° and a median value of 0.31°. For the six plate pairs with both right-lateral (RL)-slipping and left-lateral (LL)-slipping transform faults, we find that the predicted difference between RL- and LL-slipping faults is 0.91° and the observed difference is 1.41° ± 0.88° (95% confidence limits). We furthermore find that correcting transform-fault azimuths for the predicted difference between the shrinking-plate hypothesis and the rigid-plate hypothesis results in a significant improvement in fit to plate-motion data. We define a parameter γ, the fraction of predicted bias that is used to correct observed transform-fault azimuths in a plate-motion inversion. $\gamma = 0$ corresponds to the rigid-plate hypothesis, and $\gamma = 1$ corresponds to the shrinking-plate hypothesis (or more specifically, that all vertically averaged thermal stress is relieved and that transform faults parallel the relative motion of the bounding lithosphere, which generally does not move parallel to plate motion). We determine the sum-squared normalized misfit for many values of γ and find that the minimum misfit is obtained for $\gamma = 0.8 \pm 0.4$ (95% confidence limits). Thus, the rigid-plate hypothesis ($\gamma = 0$) can be rejected, while the shrinking-plate hypothesis ($\gamma = 1$) is consistent with the observed transform-fault azimuths.

The shrinking-plate hypothesis predicts horizontal shrinking of 2% Ma^{-1} for newly created lithosphere, 1% Ma^{-1} for 0.1 Ma old lithosphere, 0.2% Ma^{-1} for 1 Ma old lithosphere, and 0.02% Ma^{-1} for 10 Ma old lithosphere (Figure 1 and supporting information), which are orders of magnitude higher than the mean intraplate seismic strain rate of ~10^{-6} Ma^{-1} (5×10^{-19} s^{-1}) [*Wiens and Stein*, 1983; *Gordon*, 2000].

2. Effect of Thermal Contraction on Azimuths of Transform Faults

2.1. Introduction

A fundamental corollary of the rigid-plate hypothesis is that transform faults strike parallel to the direction of relative plate motion [*Wilson*, 1965]. If vertically averaged contractional thermal stress is fully relieved, however, lithosphere adjacent to a transform fault will have a component of velocity perpendicular to the strike of the transform fault (or, roughly equivalently, perpendicular to the direction of relative plate motion). The magnitude of this perpendicular component is approximately inversely proportional to the age of the lithosphere [*Kumar and Gordon*, 2009].

The effect of age-dependent displacement rates perpendicular to the direction of relative motion expected if plates are rigid (hereinafter "plate-motion perpendicular") is illustrated in Figure 2a. Ridge segments that separate two plates α and β are separated by a transform fault. Ridges are assumed to spread symmetrically at a half rate of $v_{1/2}$. Points on the assumed-rigid interiors of plates α and β are represented by P_α and P_β, respectively. A_α, B_α, and C_α are points along the transform-fault wall of plate α, while A_β, B_β, and C_β are the corresponding points along the transform-fault wall of plate β. $\mathbf{v}_{A\alpha}$, $\mathbf{v}_{B\alpha}$, and $\mathbf{v}_{C\alpha}$ indicate the transform-fault-perpendicular displacement rates of lithosphere in a reference frame in which point P_α, in an old portion of the same plate, is fixed and in which the median line of the corridor of lithosphere bounded by fracture zones does not rotate. $\mathbf{v}_{A\beta}$, $\mathbf{v}_{B\beta}$, and $\mathbf{v}_{C\beta}$ are the corresponding velocities for the transform-fault wall relative to the old interior of plate β.

Let $\mathbf{v}_A$ be the velocity of A_α relative to A_β. We neglect the transform-fault-parallel displacement rate due to thermal contraction as it is ≤2% of the half spreading rate [*Kumar and Gordon*, 2009]. Thus, $\mathbf{v}_A$ equals the vector sum of plate-motion-perpendicular displacement rate due to horizontal thermal contraction and a vector parallel to the transform fault with a magnitude equaling the full spreading rate (Figure 2b), i.e.,

$$\mathbf{v}_A = 2\mathbf{v}_{1/2} + \mathbf{v}_{A\alpha} - \mathbf{v}_{A\beta} \quad (1)$$

Thus, $\mathbf{v}_A$ differs from the direction of relative motion expected if plates are rigid. It is counterclockwise of the direction of rigid-plate motion for RL strike slip and clockwise for LL strike slip. If the motion between the lithosphere on either side of the transform fault is accommodated entirely by strike-slip faulting in the

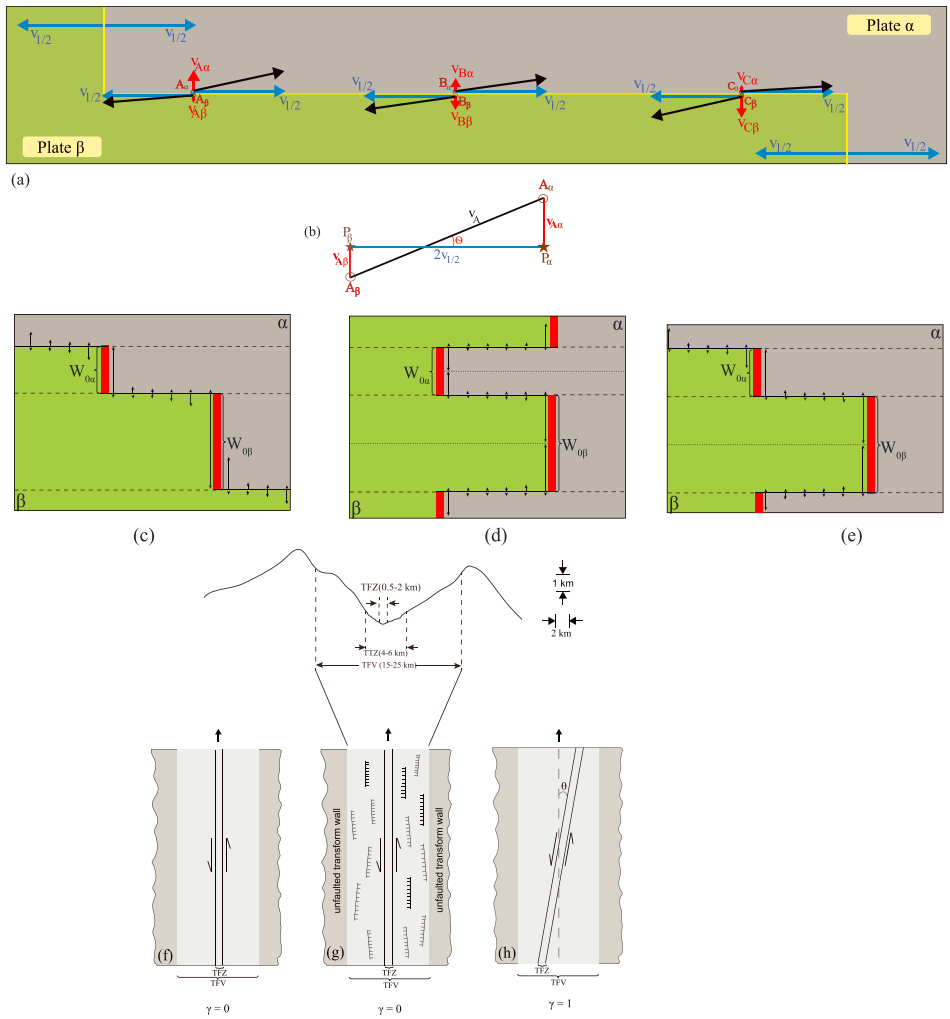

Figure 2. (a) Cartoon of velocities predicted across a transform fault after accounting for transform-perpendicular horizontal thermal contraction of oceanic lithosphere. The boundary (yellow line segments) between two plates (grey, Plate α; green, Plate β) consist of one long segment, a transform fault, and two short segments, which are segments of mid-ocean ridge orthogonal to the transform fault. Transform-fault-perpendicular velocities due to horizontal thermal contraction (red arrows) decrease approximately inversely with lithosphere age. Blue arrows, in a fixed mid-ocean ridge reference frame, show half of the relative velocity of the old interiors of the two plates. Black arrows show the resultant velocities, which are illustrated at locations A, B, and C along the transform fault. (b) Velocity space representation of the velocities across the transform fault at location A where θ is the predicted bias in transform-fault azimuth. (c–e) Cartoon illustrating the accommodation of horizontal thermal contraction for different plate boundary configurations. (Figure 2c) Stepped ridge segments: Along the transform fault enclosed by the two stepped ridge segments of lengths $W_{0\alpha}$ and $W_{0\beta}$, we assume that transform-perpendicular horizontal thermal contraction is accommodated by widening of this transform fault. The arrows represent the transform-perpendicular displacement rates of oceanic lithosphere along the transform fault. (Figure 2d) Crenelated ridge segments: We assume that transform-perpendicular horizontal thermal contraction along crenelated stepped ridge segments is accommodated by equal displacement rates of the edge of the transform valleys on either side of the crenelated corridor of lithosphere. All else being equal, the rate of widening of the transform valley is only half as large as that if the ridge segment was stepped. (Figure 2e) Hybrid ridge segment (stepped on one side and crenelated on the other): Along the side of the transform fault enclosed by the stepped ridge segment of lengths $W_{0\alpha}$, we assume that transform-perpendicular horizontal thermal contraction is accommodated entirely by widening of this transform fault. Along the side of the transform fault enclosed by the crenelated ridge segment of length $W_{0\beta}$, we assume that transform-perpendicular horizontal thermal contraction accommodated by equal displacement rates of the edge of the transform valleys on either side of the crenelated corridor of lithosphere. If $W_{0\alpha} \approx W_{0\beta}$, the rate of widening of the transform valley is approximately three fourths as large as if both ridge segments were stepped. (f–i) Hypothesized alternatives for the kinematics across a transform valley: (Figure 2f) No transform-perpendicular thermal contraction of lithosphere between transform faults; transform walls do not move perpendicular to the transform fault. The transform fault zone (TFZ) and transform tectonized zone (TTZ) are parallel to the direction of relative motion of the two assumed-rigid plates. In this case, γ is predicted to be 0 (see the text). (Figure 2g) Full transform-perpendicular contraction occurs in lithosphere between transform faults and the transform valley widens with time. In Figure 2g the slip is fully partitioned between the strike-slip faults in the TFZ and the normal faults in the walls of the transform valley. Thus, the transform fault remains parallel to the direction of relative plate motion. In this case also, $\gamma = 0$. Sketch above Figure 2g illustrates a cross section of a transform-fault valley. (Figure 2h) Full transform-perpendicular contraction occurs in lithosphere between transform faults and the transform valley widens with time. In Figure 2h no normal faulting occurs in the transform valley. Transform faults are not parallel to the relative motion of the old interiors of the plate and instead parallel the relative motion of the lithosphere immediately adjacent to the transform fault, which differs from the direction of relative plate motion of the stable plate interiors by the angle θ. In this case $\gamma = 1$.

transform fault zone (i.e., with no normal faulting in the transform-fault valley), the magnitude of θ, the local bias in transform-fault azimuth, is given by

$$|\theta| = \tan^{-1}\left(\frac{\left|\mathbf{v}_{A\alpha} - \mathbf{v}_{A\beta}\right|}{2\left|\mathbf{v}_{1/2}\right|}\right). \quad (2)$$

θ varies with the location of the point along the transform fault as it depends on the age of the lithosphere on both sides of the transform fault.

2.2. Alternative Hypotheses

Case 1:

Rigid plate: The transform-fault valley does not widen with age, and relative plate motion parallels the transform fault (Figure 2f) as is traditionally assumed in plate tectonics [*Wilson*, 1965].

If vertically averaged thermal stresses are fully relieved by thermal contraction, however, transform valleys will widen with age. We consider two further cases:

Case 2:

Shrinking plate with slip partitioned: Displacement across a transform valley is fully partitioned between normal faulting along or near the walls of the transform valley and strike-slip faulting in the valley. In this case, the transform-fault trace remains parallel to the direction of relative motion between the stable plate interiors (Figure 2g).

Case 3:

Shrinking plate with no slip partitioned: Slip due to horizontal thermal contraction may be accommodated without any normal faulting if the transform fault has a strike that is not parallel to plate motion (Figure 2h).

Let γ be the fractional multiple of bias predicted for full contraction (i.e., shrinking plate) in case 3. Thus defined, $\gamma = 0$ for cases 1 and 2 and $\gamma = 1$ for case 3.

2.3. Displacement Rates

To obtain a relationship between age and strain rate for oceanic lithosphere, we slightly modify the formulation of *Kumar and Gordon* [2009]:

$$\frac{1}{dt'}\frac{dl}{l} = -\frac{\alpha C}{t' + t_0} \quad (3)$$

where l is the length of a side of a cube of oceanic lithosphere of age t' (in Ma) undergoing isotropic thermal contraction, α is the linear coefficient of thermal expansion ($= 10^{-5}\,K^{-1}$), and t_0 is a parameter. C equals 167.2 K (see supporting information).

For simplicity, we use the same value, 0.1 Ma, for t_0 for all our calculations, which corresponds to a zero-age lithospheric thickness of ≈2 km [*Fontaine et al.*, 2008; *Kumar and Gordon*, 2009]. Analysis of gravity and topography indicates, however, that the effective elastic thickness of the lithosphere at mid-ocean ridges varies from ≈2 km for fast spreading ridges ($v \geq \approx 70\,mm\,a^{-1}$) to ≈7 km for ultraslow spreading ridges ($v \leq \approx 20\,mm\,a^{-1}$) [*Cochran*, 1979; *Luttrell and Sandwell*, 2012]. Thus, our use of a 2 km thick lithosphere is appropriate for fast spreading centers but overestimates the contraction rates at very young lithosphere for the case of ultraslow spreading (Figure 1a).

For a given value of W_0, the length of a ridge segment, and for a given value of t, the age of lithosphere undergoing isotropic thermal contraction, $W(t)$, the width of the corridor of lithosphere enclosed between a fracture zone and a transform fault is found by integrating equation (3) from $t' = 0$, when the lithosphere of interest was created, to $t' = t$, its current age, to obtain

$$W(t) = W_0\left(1 + \frac{t}{t_0}\right)^{-\alpha c}. \quad (4)$$

The transform-fault-perpendicular displacement rate of lithosphere, v_y, along one side of a transform fault is given by $\partial W/\partial t$, the rate of change of the width of the corridor of lithosphere at age t, i.e.,

$$v_y = -\frac{W_0 \alpha C}{t_0}\left(1 + \frac{t}{t_0}\right)^{-\alpha C - 1} \quad (5)$$

The transform-fault-parallel displacement rate relative to newly created lithosphere at the ridge axis, v_x, due to horizontal thermal contraction is found by integrating the strain rate of lithosphere from the ridge axis ($t = 0$) to t, the age of interest, i.e.,

$$v_x = -v_{1/2}\,\alpha C\, ln\left(1 + \frac{t}{t_0}\right) \tag{6}$$

The plate-motion-perpendicular displacement rate of lithosphere along a transform fault decreases sharply with age (Figures 1a and 1b).

2.4. Predicted Bias

2.4.1. Method

For stepped plate boundaries, we assume that thermal contraction of a corridor bounded by a fracture zone and a transform fault is accommodated by plate-motion-perpendicular displacement only along the transform fault. For a transform fault bounded by two stepped ridge segments, one with ridge-segment length of $W_{0\alpha}$ and the second with a ridge-segment length of $W_{0\beta}$ (Figure 2c), the shrinking of both adjacent fracture-zone-bound corridors of lithosphere contribute to the bias. The magnitude of the bias in transform-fault azimuth is found by substituting equation (5) into equation (2),

$$|\theta| = \tan^{-1}\left\{\frac{\alpha C}{2v_{1/2}t_0}\left[W_{0\alpha}\left(1 + \frac{t_{A\alpha}}{t_0}\right)^{-\alpha C-1} + W_{0\beta}\left(1 + \frac{t_{A\beta}}{t_0}\right)^{-\alpha C-1}\right]\right\} \tag{7}$$

where $t_{A\alpha}$ and $t_{A\beta}$, respectively, are the ages of points A_α and A_β adjacent to the transform-fault valley. The predicted bias is highest near the two ridge-transform intersections (Figure 3a). If we assume that the zero-age lithosphere thickness is 2 km for all spreading rates, as we do in the rest of this paper, then the predicted bias is larger near the ridge-transform intersections for slow spreading than for fast spreading, but about the same along most of the transform fault (Figure 3a). If instead we had used a 7 km thickness for slow spreading, the bias for slow spreading would have been calculated to be nearly identical to that for fast spreading (Figure 3a). The bias averaged over a segment that spans the entire distance between two mid-ocean ridge segments (excluding the 10 km nearest each ridge-transform intersection) is 0.72° for a 2 km initial thickness and is 0.61° for a 7 km initial thickness. Thus, in this paper the predicted bias for ultraslow spreading is overestimated by ≈ 18%. Along most transform faults, the amount overestimated will be smaller than this, especially if the insonified portion of the segment ends more than 10 km from the ridge-transform intersection or if the spreading rate exceeds ≈ 20 mm a^{-1}.

The sense of the bias correction for a given transform fault depends on the sense of slip along the transform fault. For RL slip, the bias is predicted to be counterclockwise, and for LL slip, it is predicted to be clockwise. Azimuths for RL-slipping transform faults, which are measured clockwise relative to north, must be increased to remove the bias. In contrast, the azimuths of LL-slipping transform faults must be decreased to remove the bias. With these sign conventions, the bias for a RL-slipping transform fault is negative, while that for a LL-slipping transform fault is positive.

If spreading is assumed to be symmetric and its rate constant in time, the age of a point adjacent to a transform fault is its distance from the corresponding ridge axis divided by the half spreading rate. Thus, equation (7) can be rewritten as

$$|\theta| = \tan^{-1}\frac{\alpha C}{2v_{1/2}t_0}\left[W_{0\alpha}\left(1 + \frac{x_{A\alpha}}{v_{1/2}t_0}\right)^{-\alpha C-1} + W_{0\beta}\left(1 + \frac{x_{A\beta}}{v_{1/2}t_0}\right)^{-\alpha C-1}\right] \tag{8}$$

where $x_{A\alpha}$ and $x_{A\beta}$ are the distances of adjacent points (but on opposite sides of the transform fault) from their respective mid-ocean ridge axes.

Predicted plate-motion-perpendicular displacement rates for crenelated ridge segments are half as large as those for stepped ridge segments because we assume that displacement due to the contraction of a corridor of lithosphere bounded by a crenelated ridge segment is equally divided between its two adjacent transform faults (Figure 2d). For a transform fault bounded by two crenelated ridge segments, the bias is thus half of that for a transform fault bounded by two stepped ridge segments. For a transform fault bounded by a stepped ridge segment on one side and a crenelated ridge segment on the other, the bias is three fourths of that for a transform fault bounded by two stepped ridge segments (Figure 2e).

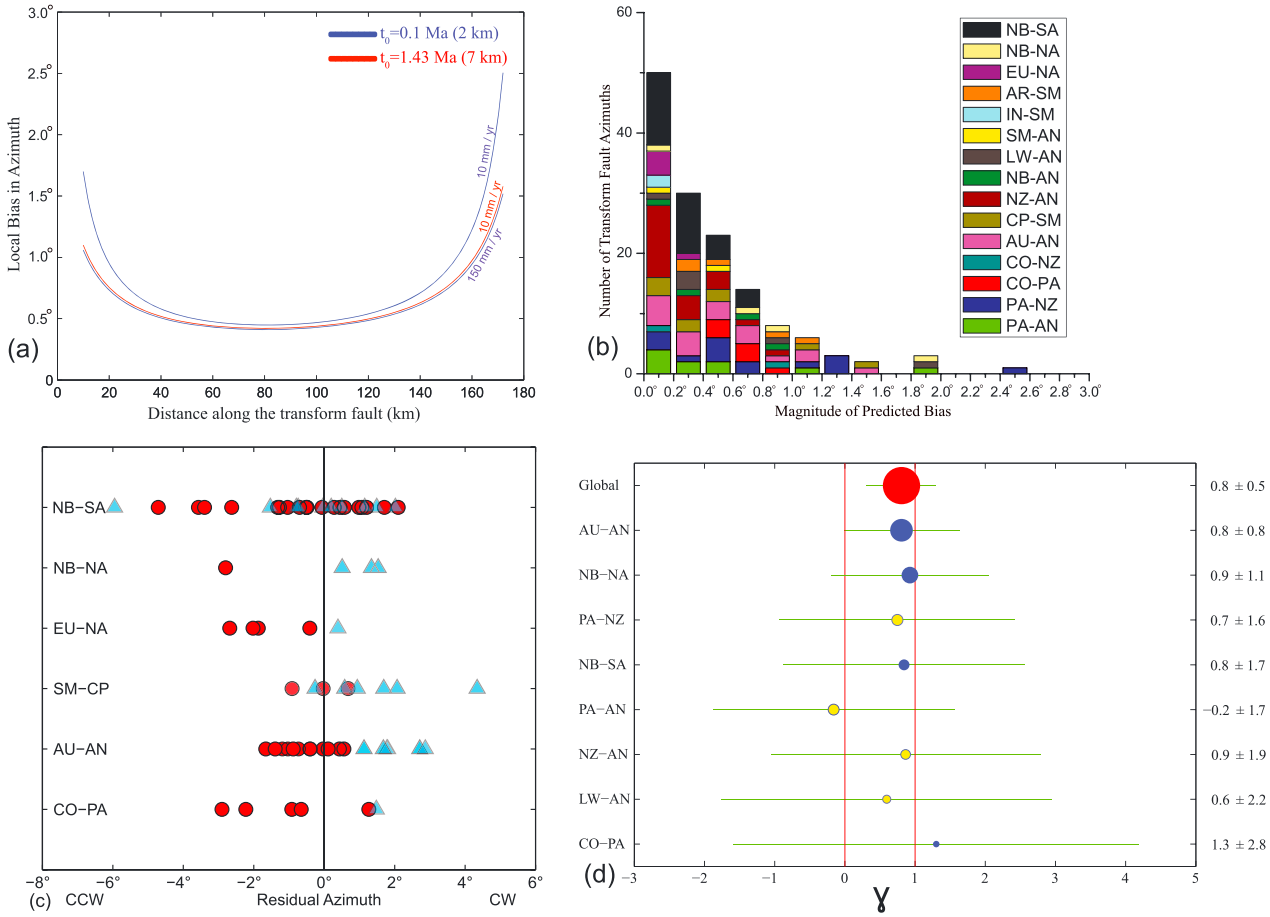

Figure 3. (a) Bias in transform-fault azimuth predicted along the Wilkes transform fault (along the Pacific-Nazca plate boundary) as a function of distance from the ridge axis for hypothetical full spreading rates of 10 mm a^{-1} and 150 mm a^{-1}. The length of the Wilkes transform fault is 182 km. It is bounded by stepped segments of mid-ocean ridge on both sides, and the lengths of the adjacent ridge segments are 344 km and 534 km. (b) Distribution of predicted biases averaged over the insonofied lengths used to estimate the 139 transform-fault azimuths analyzed herein (Table S1 in the supporting information). Plate name abbreviations: AN, Antarctica; AR, Arabia; AU, Australia; CO, Cocos; CP, Capricorn; EU, Eurasia; IN, India; LW, Lwandle; NA, North America; NB, Nubia; NZ, Nazca; PA, Pacific; SA, South America; SM, Somalia. (c) Residuals with respect to the best fitting angular velocity for each plate pair having both left-lateral-slipping (blue Δ) and right-lateral-slipping (red O) transform faults. Abbreviations: AN, Antarctica; AU, Australia; CO, Cocos; CP, Capricorn; CW, clockwise; CCW, counterclockwise; EU, Eurasia; NA, North America; NB, Nubia; PA, Pacific; SA, South America; SM, Somalia. For each plate pair, the mean residual of left-lateral-slipping faults is clockwise of that for right-lateral-slipping faults. (d) The parameter γ estimated from only transform-fault azimuths (i.e., no spreading rates) for the 12 individual plate pairs (blue or yellow) with the smallest uncertainties: blue if both right-lateral- and left-lateral-slipping transform faults occur along their mutual boundary; yellow if transform faults slip in only one sense along their mutual boundary. Green line segments show the 95% confidence limits. The estimate from combining all data (red) is consistent with $\gamma = 1$ and excludes $\gamma = 0$.

2.4.2. Results

The bias predicted for the transform-fault azimuths that we analyzed varies in magnitude from 0.01° to 2.44° with the mean and median values of the magnitude of the predicted bias being 0.46° and 0.31°, respectively. Only 15 transform-fault azimuths have predicted biases exceeding 1.0° (Figure 3b and Table S1). The greatest biases are predicted for transform-fault segments for which the adjacent ridge segments are long and the bathymetric data are collected near a ridge-transform intersection (Figures 3a, 4b, and 4d). Predicted biases depend only weakly on spreading rate and tend to decrease with increasing length of a transform fault (Figures 4a and 4c).

2.4.3. Bias for Plate Pairs With Both Right-Lateral- and Left-Lateral-Slipping Transform Faults

Six plate pairs have both RL- and LL-slipping transform faults along their mutual boundaries. As shown above, the shrinking-plate hypothesis predicts that RL-slipping transform faults will be biased counterclockwise of the plate-motion direction (Figure 2), tending to result in negative residuals, while LL-slipping faults will be biased clockwise of the direction of plate motion, tending to result in positive residuals. The mean bias for

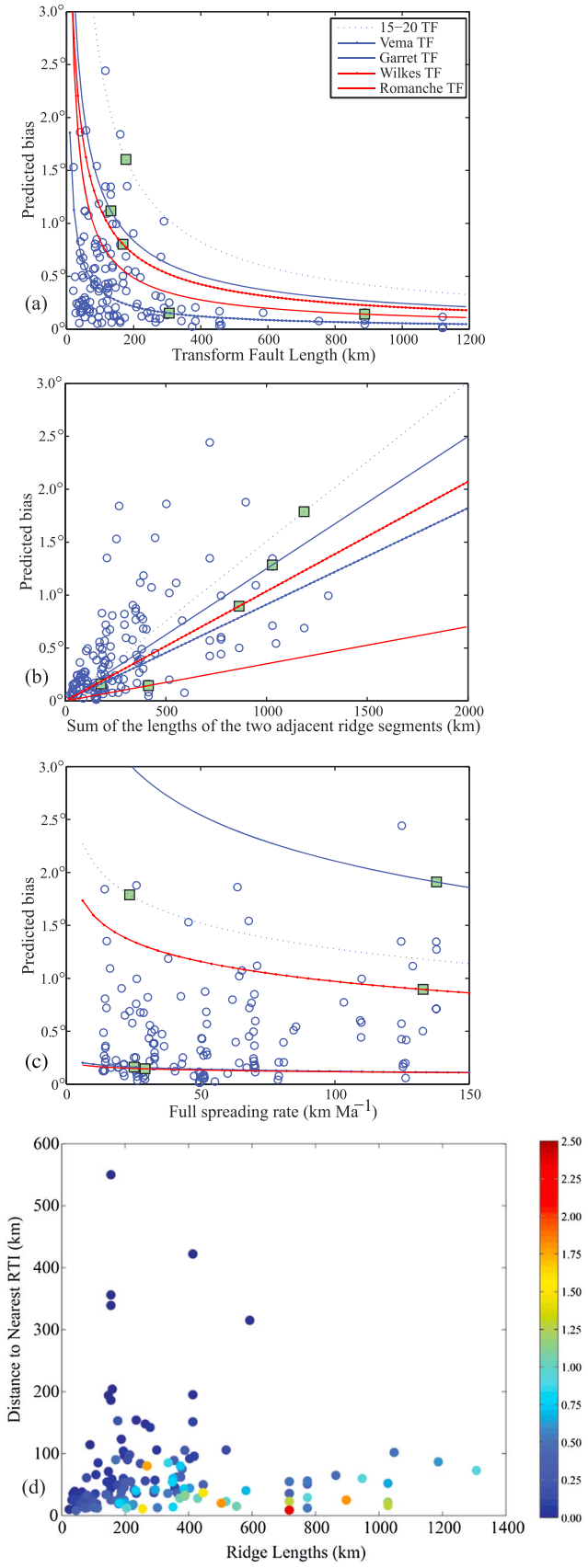

Figure 4. (a) Predicted bias (circles) versus transform-fault length for the 139 azimuths of transform faults analyzed herein. Reference curves show predicted bias averaged along an entire transform fault as a function of transform-fault length for five transform faults while holding the ridge segment lengths and the spreading rates fixed at their observed values. Squares: fault-averaged bias predicted for the observed length for each of the five transform faults. (b) Predicted bias (circles) versus the sum of the lengths of the adjacent segments of mid-ocean ridge. Only half the length of a ridge segment is used if it is crenelated. Reference curves show predicted bias averaged along the entire transform fault for the same five transform faults as in Figure 4 a while holding the transform-fault lengths and spreading rates fixed at their observed values. Squares: fault-averaged bias for the observed sum of ridge-segment lengths for each of the five transform faults. (c) Predicted bias (circles) versus spreading rate. Reference curves show predicted bias averaged along an entire transform fault as a function of spreading rate for the same five transform faults as in Figures 4a and 4b while holding the ridge-segment lengths and the transform-fault lengths fixed at their observed values. Squares: fault-averaged bias predicted for the observed spreading rate for each of the five transform faults. (d) Distance of the midpoint of each insonified segment of a transform fault from the nearest ridge-transform intersection (RTI) versus the sum of the lengths of the adjacent segments of mid-ocean ridge. Only half the length of a ridge segment is used if it is crenelated. The color of each circle indicates the size of the predicted bias in degrees. Most of the higher values of bias result from a combination of a distance to the nearest RTI $<$ ≈125 km and a ridge-length sum $>$ ≈180 km.

LL-slipping faults for six plate pairs is predicted to be 0.54° and the mean bias for RL-slipping faults is predicted to be −0.37° (where clockwise is positive). The difference between these is 0.91° (Table 1).

These predicted biases and predicted differences can be compared with the residuals observed for faults between these six pairs for which the mean residual for LL-slipping faults is 0.65° ± 0.76° (95% confidence limits) and for which the mean residual for right-lateral-slipping faults is −0.76° ± 0.43° (95% confidence limits). The difference between these is 1.41° ± 0.88° (95% confidence limits)

Table 1. Predicted Mean Biases and Observed Mean Residuals[a]

	N							
Plate Pair	LL	RL	LL[b]	RL[b]	Δ[b]	LL[c]	RL[c]	Δ[c]
CO-PA	1	5	0.77°	−0.63°	1.40°	1.48°	−1.09°	2.57°
AU-AN	7	12	0.60°	−0.45°	1.05°	1.05°	−0.55°	1.66°
CP-SM	6	3	0.64°	−0.42°	1.06°	1.56°	−0.09°	1.65°
EU-NA	1	4	0.16°	−0.17°	0.33°	0.39°	−1.75°	2.14°
NB-NA	3	1	0.92°	−0.99°	1.91°	1.13°	−2.80°	3.93°
NB-SA	10	19	0.36°	−0.26°	0.62°	0.37°	−0.60°	0.97°
Total (*N*) or Mean	28	44	0.54°	−0.37°	0.91°	0.65° ± 0.76°	−0.76° ± 0.43°	**1.41° ± 0.88°**

[a]Results are shown for the six plate pairs having both right-lateral-slipping and left-lateral-slipping transform faults along their mutual boundary. Abbreviations: *N*, number of transform-fault segments; LL, left-lateral-slipping fault; RL, right-lateral-slipping fault; Δ, mean bias (or mean residual) of left-lateral-slipping faults minus that for right-lateral-slipping faults; CO, Cocos plate; PA, Pacific plate; AU, Australia plate; AN, Antarctica plate; CP, Capricorn plate; SM, Somalia plate; EU, Eurasia plate; NA, North America plate; NB, Nubia plate; SA, South America plate. Quoted uncertainties are 95% confidence limits and were determined by linear propagation of errors of the uncertainties assigned to individual azimuths of transform-fault segments. The overall mean difference (with its 95% confidence limits) for the six plate pairs combined is shown in bold.
[b]Predicted bias.
[c]Observed residuals.

(Table 1 and Figure 3c; cf. Figure S2). In each case the observed value differs significantly from zero (the prediction for rigid plates), but insignificantly from the values predicted for the shrinking-plate hypothesis. For all six plate pairs, the mean residual (with respect to values calculated from the best fitting angular velocity fit to all data in the plate pair) for LL-slipping faults is greater than (i.e., clockwise of) the mean residual for RL-slipping faults. As with a coin flip, the odds of this occurring by chance for all six plate pairs are merely 1 in 64.

Cocos-Pacific and Nubia-North America, which are the two plate pairs predicted to have the largest difference between LL- and RL-slipping faults, also have the largest observed difference between LL- and RL-slipping faults (Table 1).

3. Global Analysis

3.1. Methods

The procedure for testing whether transform-fault azimuths are better fit assuming a rigid plate or a shrinking plate consists of the following steps: (i) The bias in azimuth, taken to be the local bias (from equation (8)) averaged over the insonified portion of the transform fault, is predicted for each transform-fault segment for which azimuth estimates are available. Lengths of ridge segments, lengths of transform faults, and distances of midpoints of insonified sections of transform faults [*DeMets et al*., 2010] from ridge axes were measured using a map of 1 min resolution global topography version 12.1 of *Smith and Sandwell* [1997]. Slip rate along a transform fault is determined from the best fitting angular velocity for the relevant plate pair [*DeMets et al*., 2010]. (ii) The bias correction is added to observed transform-fault azimuths, and the sum-squared normalized misfit is determined using the same least squares method used by *DeMets et al*. [2010]. For each plate pair we consider two data sets, one consisting of only the transform-fault azimuths, and a second consisting of both transform-fault azimuths and spreading rates (after correction for outward displacement [*DeMets and Wilson*, 2008; *DeMets et al*., 2010]). (iii) Step (ii) is repeated many times for many closely spaced values of γ over a range wide enough to locate the best fitting value and 95% confidence limits of γ. (iv) Step (iii) is repeated for each plate pair. (v) The results from all plate pairs are combined to find the best global estimate and uncertainty for γ. γ_m, our best estimate of γ, is the value of γ that results in the smallest sum-squared normalized misfit.

3.2. Data

Of the 28 plate pairs included in the MORVEL analysis that are separated in part or whole by mid-ocean ridge segments [*DeMets et al*., 2010], we analyzed data for the 15 plate pairs best populated with transform-fault data (Pacific-Antarctica, Cocos-Pacific, Pacific-Nazca, Cocos-Nazca, Nazca-Antarctica, Nubia-South America, Europe-North America, Nubia-North America, Somalia-Capricorn, India-Somalia, Nubia-Antarctica, Somalia-Antarctica, Lwandle-Antarctica, Arabia-Somalia, and Australia-Antarctica) (Table S1).

Table 2. γ_m for All the Plate Pairs[a]

	Both Spreading Rates and TF Azimuths				TF Azimuths Only			
Plate Pair	*N*	γ_m	χ^2 ($\gamma = 0$)	χ^2 ($\gamma = 1$)	*N*	γ_m	χ^2 ($\gamma = 0$)	χ^2 ($\gamma = 1$)
AU-AN	186	0.8 ± 0.8	181.0	178.3	19	0.8 ± 0.8	19.2	15.8
NB-NA	165	1.3 ± 1.0	175.6	169.3	4	0.9 ± 1.1	3.1	0.3
NB-SA	128	0.3 ± 1.3	116.5	116.9	29	0.8 ± 1.7	26.3	25.1
PA-NZ	57	1.0 ± 1.6	56.8	55.3	15	0.7 ± 1.6	5.8	5.3
PA-AN	58	-0.4 ± 1.7	52.7	55.2	10	-0.2 ± 1.7	5.6	7.3
NZ-AN	86	1.1 ± 1.9	82.6	81.5	21	0.9 ± 1.9	25.1	24.3
LW-AN	29	0.6 ± 2.2	14.0	13.9	6	0.6 ± 2.2	1.0	0.8
SM-CP	65	2.2 ± 2.9	58.2	59.6	9	1.9 ± 4.3	4.4	3.8
CO-PA	67	1.2 ± 2.8	72.6	72.0	6	1.3 ± 2.8	1.6	0.9
AR-SM	56	1.0 ± 3.0	51.9	51.4	5	4.1 ± 9.3	2.6	2.4
NB-AN	83	-3.3 ± 3.6	78.5	80.6	4	2.6 ± 6.3	0.4	0.2
SM-AN[b]	63	-0.8 ± 3.7	25.7	26.4	2	N/A	N/A	N/A
CO-NZ[b]	90	3.0 ± 4.0	89.9	88.7	2	N/A	N/A	N/A
EU-NA	459	12.2 ± 6.5	481.6	479.6	5	9.3 ± 11.0	3.4	2.8
IN-SM[b]	115	-22.4 ± 78.6	112.4	112.5	2	N/A	N/A	N/A
Combined	1707	0.8 ± 0.4	1650.0	1641.3	139	0.8 ± 0.5	98.5	89.0

[a] $\gamma_m = 0$ is expected if plates are rigid; $\gamma_m = 1$ is expected if the azimuths of transforms are affected by horizontal contraction of the lithosphere as proposed by *Kumar and Gordon* [2009]. Uncertainties are 95% confidence limits. Abbreviations: *N*, number of data; AN, Antarctica; AR, Arabia; AU, Australia; CO, Cocos; CP, Capricorn; EU, Eurasia; IN, India; LW, Lwandle; NA, North America; NB, Nubia; NZ, Nazca; PA, Pacific; SA, South America; SM, Somalia; TF, transform fault; N/A, not applicable.
[b] These plate pairs have only two observed azimuths of transform faults.

The data that we analyze are identical to those of MORVEL [*DeMets et al*., 2010] except for three transform-fault azimuths along the Central Indian Ridge. (1) We omit the azimuth of the Vema transform fault. *DeMets et al*. [2005] showed that the Vema transform fault does not record motion between the Somalia and Capricorn plates, but between the Somalia plate, on the one hand, and the deforming zone between the Indian and Capricorn plates, on the other hand. (2) We correct the location assigned to the transform-fault azimuth of transform-fault "O" [*Royer et al*., 1997] (Table S1). (3) *DeMets et al*. [2010] use an azimuth for the Argo transform fault determined by *Parson et al*. [1993] from GLORIA side-scan sonar data, which we expect to give high resolution and accurate results. This azimuth unexpectedly differs by 5.6° from that inferred from the lower resolution satellite-derived gravity data [*Smith and Sandwell*, 1997]. This difference is larger than anywhere else on the planet; the azimuth from *Parson et al*. [1993] is inconsistent with other data along the Central Indian Ridge. We chose to use the azimuth inferred from gravity.

Twelve of the 15 plate pairs that we analyzed have three or more transform-fault azimuths, which is the minimum required to estimate γ from only transform-fault azimuths. The other three plate pairs have only two transform-fault azimuths and are incorporated when we also include spreading rates.

3.3. Results

When only transform faults are analyzed (with no spreading rates), the plate pairs that best constrain γ (those with both LL- and RL-slipping transform faults) favor a value near one (Figure 3d). When all plate pairs are combined, γ_m determined from only transform-fault azimuths is 0.8 ± 0.5 (95% confidence limit) (Table 2 and Figure 3d). γ_m determined from transform-fault azimuths combined with spreading rates is 0.8 ± 0.4 (95% confidence limits) (Table 2 and Figure S1). The bias correction improves the fit for all six plate pairs having both LL- and RL-slipping transform faults (Table 2 and Figure 3d).

4. Examples

4.1. 100°E Transform Fault Along the Southeast Indian Ridge (Australia-Antarctica Plate Boundary)

The Australia-Antarctica plate boundary along the Southeast Indian Ridge is populated with both RL- and LL-slipping transform faults (Figure 5a). The residuals from LL-slipping transform faults tend to lie about 2° clockwise of residuals from RL-slipping transform faults, which is slightly larger than, but consistent with, the predicted difference of 1.05° (Table 1).

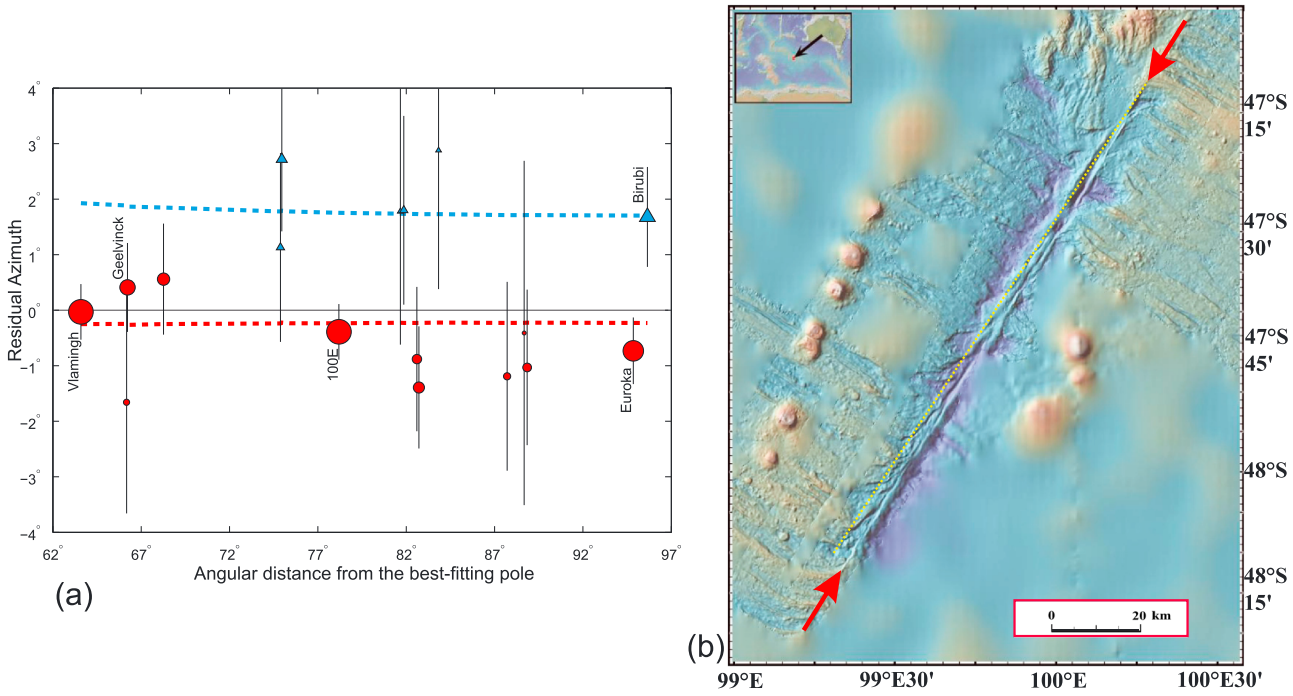

Figure 5. (a) Transform-fault azimuths (measured clockwise from north) along the Australia-Antarctica plate boundary from *DeMets et al*. [2010] (except that we have omitted the Tasman transform fault, which lies adjacent to the Australia-Macquarie diffuse plate boundary, and the 96.15°E transform fault, the strike of which is poorly constrained). Blue triangles, residual azimuths (with respect to the best fitting angular velocity of *DeMets et al*. [2010]) of left-lateral (LL)-slipping transform faults; red circles, residual azimuths of right-lateral (RL)-slipping faults. The blue dashed curve is fit to spreading rate data plus azimuths of LL-slipping faults; the red dashed curve is fit to spreading rate data plus azimuths of RL-slipping faults. The residual azimuths of LL-slipping faults tend to be ≈2° clockwise of the residual azimuths of RL-slipping faults. (b) GeoMapApp [*Ryan et al*., 2009] image of the 100.0°E transform fault along the Australia-Antarctica plate boundary. The red arrows show our best estimate of the overall strike (032.0°) of the RL-slipping 100.0°E transform fault. The yellow dotted line shows the strike predicted (033.6°) for the 100.0°E transform from the estimated strikes of the LL-slipping fault segments (i.e., from the blue dashed curve in Figure 5a). The difference of 1.6° is approximately that expected from the horizontal thermal contraction of oceanic lithosphere. Mercator's projection.

In Figure 5b the red arrows show our best estimate of the overall strike (032.0°) of the RL-slipping 100.0°E transform fault, which is 0.5° clockwise of the strike (031.5°) adopted by *DeMets et al*. [2010]. Both of these are counterclockwise of the strike predicted (033.6°, yellow dotted line) for the 100.0°E transform from the estimated strikes of the LL-slipping fault segments along the Australia-Antarctica plate boundary. The difference of 1.6° from our best estimate is near that expected from the horizontal thermal contraction of oceanic lithosphere.

4.2. Clipperton Transform Fault Along the East Pacific Rise (Cocos-Pacific Plate Boundary)

The plate-motion data along the Cocos-Pacific plate boundary along the East Pacific Rise include two RL-slipping transform faults and one LL-slipping transform fault (Figure 6a). The azimuth of the RL-slipping Orozco transform fault is ≈1° counterclockwise of the azimuth calculated from the best fitting angular velocity (i.e., the one that best fits all the data along the Pacific-Cocos boundary). Similarly, the four azimuths along the RL-slipping Siquieros transform fault are on average ≈1° counterclockwise of the calculated azimuths. In contrast, the azimuth of the LL-slipping Clipperton transform fault is ≈1° clockwise of its calculated azimuth.

In Figure 6b the blue arrows indicate our best estimate of the overall strike of the Clipperton transform fault zone (081.3°), which differs slightly from the value of 082° estimated by *Gallo et al*. [1986] and adopted by *DeMets et al*. [2010]. The 0.7° difference between the value shown in Figure 6b and that of *Gallo et al*. [1986] is mainly the difference between the ≈082° strike of individual segments (separated by extensional relay zones) and the overall strike of the segments considered together (Figure 6b). The red dotted line shows the strike predicted (079.9°) for the Clipperton transform fault from the strikes of the RL-slipping Pacific-Cocos fault segments (Figure 6b). The difference of 1.4° is about that expected from the horizontal thermal contraction of oceanic lithosphere.

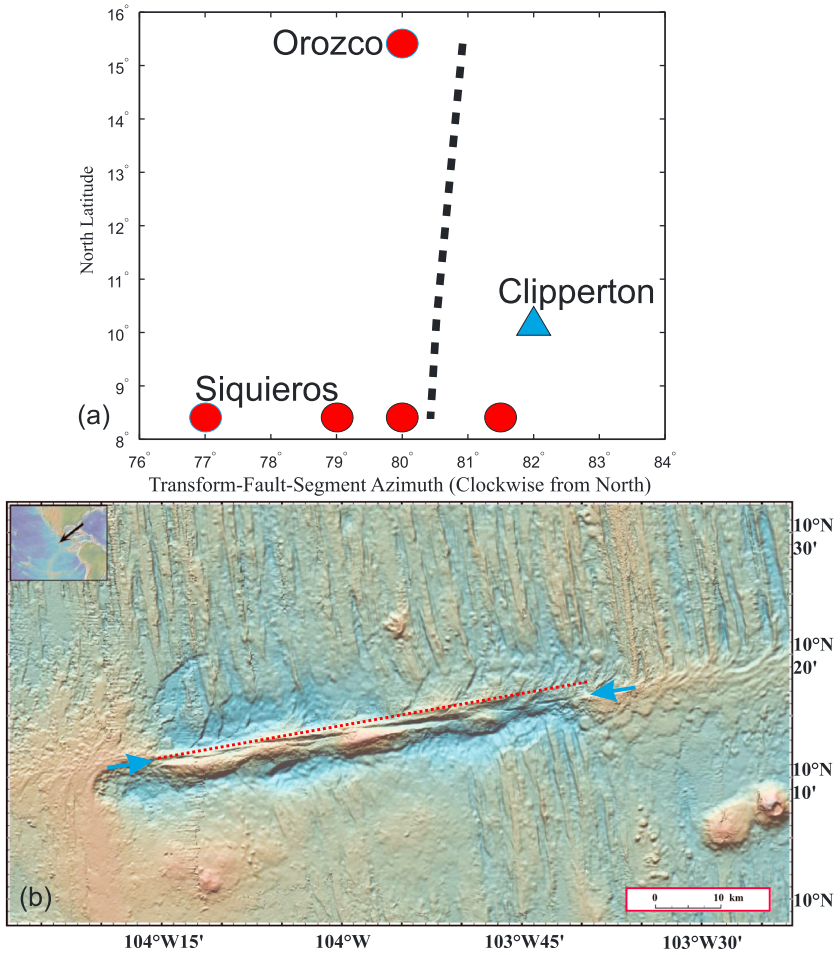

Figure 6. (a) Transform-fault azimuths (measured clockwise from north) along the Pacific-Cocos plate boundary from *DeMets et al*. [2010]. Blue triangle, azimuth of left-lateral (LL)-slipping Clipperton transform fault; red circles, azimuth of the right-lateral (RL)-slipping faults segments along the Orozco and Siquieros transform faults. The azimuth of the LL-slipping fault is clockwise of the average azimuth of the RL-slipping fault segments. The black dashed curve shows azimuths calculated from the angular velocity that best fits all the observed data from only this plate pair [*DeMets et al*., 2010]. (b) GeoMapApp [*Ryan et al*., 2009] image of the Clipperton transform fault along the Pacific-Cocos plate boundary. The blue arrows shows our best estimate of the overall strike (081.3°) of the Clipperton transform fault. The red dotted line shows the strike (079.9°) predicted for the Clipperton transform from the estimated strikes of the RL-slipping fault segments. The difference of 1.4° is approximately that expected from the horizontal thermal contraction of oceanic lithosphere. Mercator's projection.

4.3. Kane Transform Fault Along the Mid-Atlantic Ridge (Nubia-North America Plate Boundary)

The plate-motion data along the Nubia-North America boundary along the Mid-Atlantic Ridge include three LL-slipping transform faults and one RL-slipping transform fault (Figure 7a). The azimuths of the LL-slipping Oceanographer, Hayes, and Atlantis transform faults are, on average, ≈1° clockwise of the azimuths calculated from the best fitting angular velocity. In contrast, the azimuth of the RL-slipping Kane transform fault is ≈2.5° counterclockwise of the calculated azimuth.

In Figure 7b, the magenta arrows indicate our best estimate of the overall strike of the Kane transform fault zone (098.5°), which is identical to that estimated by *Roest et al*. [1984] for the overall strike of the Kane transform-fault from GLORIA data. It differs, however, by 0.5° from the value of 098° estimated by *Pockalny et al*. [1988] from Seabeam data and differs by 0.5° from the value of 099.0° adopted by *DeMets et al*. [2010]. The black dotted line shows the strike predicted (103.1°) for the Kane transform from the estimated strikes of the LL-slipping North America-Nubia fault segments (Figure 7b). The difference of 4.6° is in the

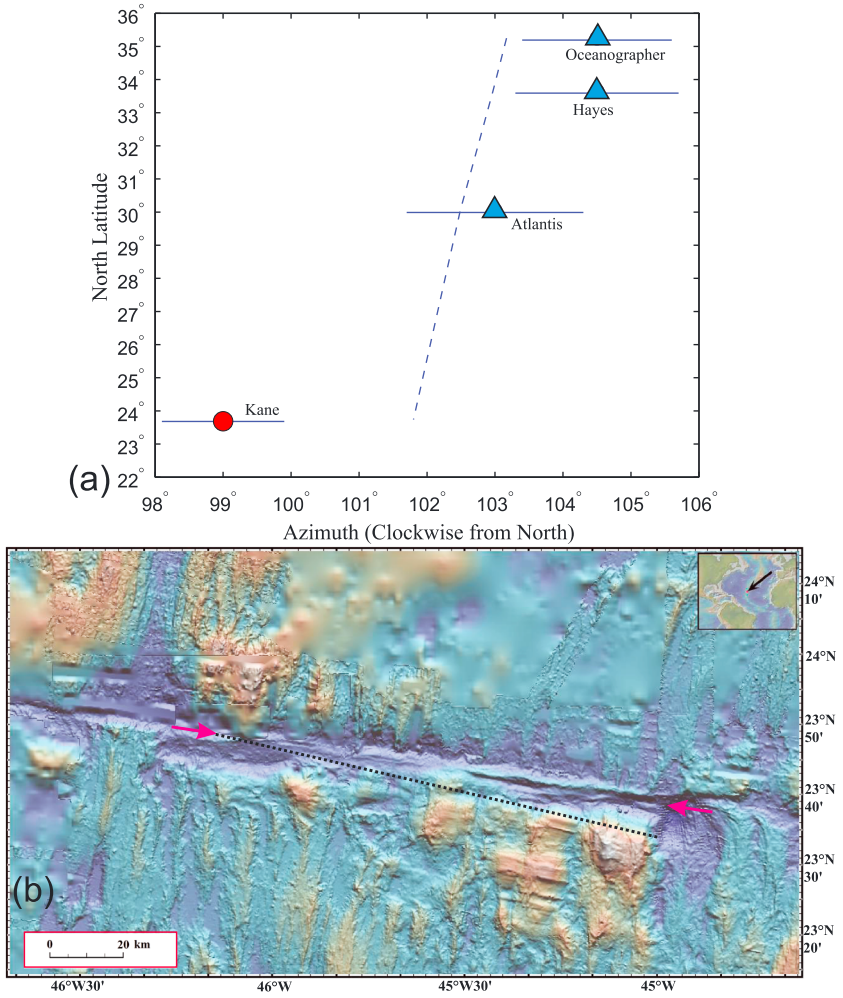

Figure 7. (a) Transform-fault azimuths (measured clockwise from north) along the North America-Nubia plate boundary from *DeMets et al*. [2010]. Blue triangles, azimuths of left-lateral (LL)-slipping transform faults; red circle, azimuth of the right-lateral (RL)-slipping Kane transform fault. The azimuths of the LL-slipping faults are clockwise of the azimuth of the RL-slipping fault. The blue dashed curve shows azimuths calculated from the angular velocity that best fits all the observed data from only this plate pair [*DeMets et al*., 2010]. (b) GeoMapApp [*Ryan et al*., 2009] image of the Kane transform fault along the North America-Nubia plate boundary. The magenta arrows show our best estimate of the overall strike (098.5°) of the Kane transform fault. The black dotted line shows the strike predicted (103.1°) for the Kane transform from the estimated strikes of the LL-slipping fault segments. The difference of 4.6° is in the correct sense but larger than that expected from the horizontal thermal contraction of oceanic lithosphere. Mercator's projection.

correct sense of, but greater in magnitude than, that expected from the horizontal thermal contraction of oceanic lithosphere. The difference between LL- and RL-slipping faults along the Nubia-North America boundary is expected to be 1.9° (Table 1). Thus, about half of the discrepancy can be explained by horizontal thermal contraction. If the diffuse plate boundary between the North and South America plates along the Mid-Atlantic Ridge continues south of the Kane transform fault, some of the difference between observed and predicted strike of the Kane transform might be due to distributed deformation accommodated in this diffuse plate boundary [*DeMets et al*., 1990; *Gordon*, 1998].

5. Discussion

A prediction of the shrinking-plate hypothesis is that the azimuths of LL-slipping transform faults should differ subtly from those of RL-slipping transform faults. The global analysis of the strikes of transform faults reveals a previously unsuspected significant difference between the azimuths of LL- and RL-slipping faults.

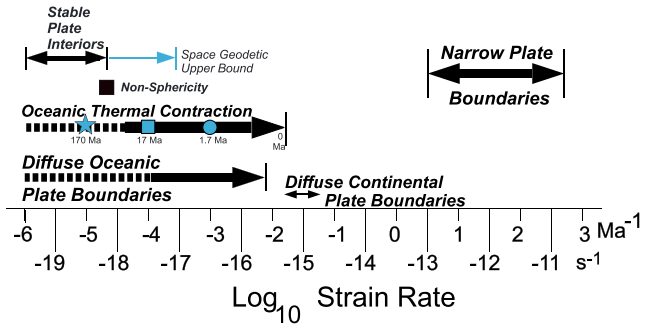

Figure 8. Range of spatially averaged strain rates for selected tectonic processes. The lower bound for strain rate of stable plate interiors is the mean seismic strain rate estimated from oceanic seismic moment release [*Wiens and Stein*, 1983; *Gordon*, 1998]. Space geodetic data provide an upper bound [*Argus and Gordon*, 1996; *Dixon et al*., 1996; *Argus et al*., 2010], but in the figure we emphasize a lower upper bound estimated herein for plate motion over a nonspherical Earth [*McKenzie*, 1972; *Turcotte and Oxburgh*, 1973]. Strain rates from narrow plate boundaries and diffuse oceanic plate boundaries are from *Gordon* [1998, 2000] and those for diffuse continental plate boundaries from *England and Molnar* [1997] and *Davies et al*. [1997].

This new evidence strongly favors the shrinking-plate hypothesis over the rigid-plate hypothesis. Thus, we infer that plates are not rigid, although plate rigidity remains a useful approximation.

Korenaga [2007] questioned earlier evidence that the lithosphere contracts freely in response to horizontal thermal contraction. He instead proposes a thermal cracking model wherein thermal stresses are dissipated by widespread tensional cracking in shallow lithosphere. He argues that thermal stress release by cracking is localized, and thus, thermal cracking should be present everywhere in oceanic lithosphere. As far as we know, the tensional cracking postulated by *Korenaga* [2007] has not been observed anywhere. His model predicts no net horizontal contraction of the lithosphere between transform faults or fracture zones and thus predicts the same azimuth for a transform fault as does the assumption of rigid plates. Thus, our results contradict the predictions of his model.

Instead, transform faults (and possibly other elements of the transform valley as well) serve to relieve much of the vertically averaged thermoelastic stress in young oceanic lithosphere and appear to do so for a wide range of lengths of mid-ocean-ridge segments (Figure 4b). If part of the widening of transform-fault valleys is also accommodated by normal faulting in the valley walls [*Wilcock et al*., 1990] and other processes that thin the lithosphere in the transform-fault valley, then the lithosphere of the transform valley may be weaker than adjacent lithosphere. With $\gamma_m = 0.8 \pm 0.4$, it follows that the fraction of widening accommodated by normal faulting is 0.2 ± 0.4 (95% confidence limits).

Although transform faults do not precisely parallel plate motion, that the mean bias is merely 0.46° indicates that the effect on estimated directions of plate motion is small, all the more so for plate boundaries with both LL- and RL-slipping transform faults, for which the bias has opposite signs and will partly cancel out in estimates of relative plate velocity [e.g., *DeMets et al*., 1990, 1994, 2010].

Our results constrain the magnitude of intraplate horizontal strain and the relative roles of some of the processes that may contribute to it. The model of *Kumar and Gordon* [2009] predicts strain rates in young (≤17 Ma old) lithosphere ranging from ≈2% Ma^{-1} for newly created lithosphere to ≈10^{-4} Ma^{-1} for 17 Ma old lithosphere (Figure 8 and supporting information). Thermal contractional strain rates in young oceanic lithosphere are orders of magnitude greater than the average oceanic seismically released strain rate of 10^{-6} Ma^{-1} (lower bound on strain rate of stable plate interiors as shown in Figure 8), but orders of magnitude lower than strain rates averaged across narrow plate boundaries, which range from ≈3 to ≈10^3 Ma^{-1} (Figure 8) [*Gordon*, 1998, 2000]. Thermal contractional strain rates in very young oceanic lithosphere are comparable to strain rates in diffuse oceanic plate boundaries and overlap the strain rates for diffuse continental plate boundaries (Figure 8) [*Gordon*, 1998, 2000].

Another cause of intraplate strain is that of the movement of tectonic plates over a nonspherical Earth [*McKenzie*, 1972; *Turcotte and Oxburgh*, 1973]. *McKenzie* [1972] estimates that strains of ~1% are produced in a plate the size of the Pacific plate when it moves through 90° of latitude. The youngest (32 Ma) well-constrained Pacific plate paleomagnetic pole is located at 83.5°N, 44.6°E [*Horner-Johnson and Gordon*, 2010], which indicates an average rate of northward motion of the Pacific plate of ≈0.2° per Ma. At that rate it would take ≈450 Ma for the Pacific plate to move through 90° of latitude indicating an average strain rate of ≈2×10^{-5} Ma^{-1} (= 1%/(450 Ma)) as shown in Figure 8. This is similar to the thermal contractional strain rate that we predict for 80 Ma old lithosphere. Thus, for the Pacific plate, straining from movement over a

nonspherical Earth is less than the thermal contractional straining for lithosphere younger than ≈80 Ma, comparable for lithosphere with an age near 80 Ma, and exceeds the thermal contractional straining for lithosphere older than ≈80 Ma. All else being equal, for plates smaller than the Pacific plate, the straining due to motion over a nonspherical Earth is less important.

6. Conclusions

1. Inconsistent with the rigid-plate hypothesis, but as predicted by the shrinking-plate hypothesis, observed transform azimuths differ significantly between RL- and LL-slipping faults along a common plate boundary. Thus, transform-fault azimuths do not precisely parallel the direction of relative plate motion.
2. Other hypotheses that predict no widening of transform valleys [e.g., *Korenaga*, 2007] can also be rejected.
3. These new results validate the predictions of the shrinking-plate hypothesis, which indicates horizontal shrinking rates of 2% Ma^{-1} for newly created lithosphere, 1% Ma^{-1} for 0.1 Ma old lithosphere, 0.2% Ma^{-1} for 1 Ma old lithosphere, and 0.02% Ma^{-1} for 10 Ma old lithosphere, which are orders of magnitude higher than the mean intraplate seismic strain rate of ~10^{-6} Ma^{-1} (5×10^{-19} s^{-1}).
4. At least 40% of the widening of transform-fault valleys results in an azimuth that differs from that expected if the plates were rigid. Within uncertainties, some (≤60%) of the predicted widening of the transform-fault valley could be accommodated by normal faulting in the walls of the valley [e.g., *Wilcock et al*., 1990].
5. Horizontal thermal contraction [*Kumar and Gordon*, 2009; *Kreemer and Gordon*, 2014] of oceanic lithosphere younger than ≈ 80 Ma results in the largest strain rates in plate interiors. Strain rates due to plate movement over a nonspherical Earth [*McKenzie*, 1972; *Turcotte and Oxburgh*, 1973] may be larger, however, in continental lithosphere and in old (>80 Ma) oceanic lithosphere.
6. Thermal contraction rates in young oceanic lithosphere are comparable to the highest strain rates in diffuse oceanic plate boundaries.

Acknowledgments

We thank Ben Horner-Johnson for his help with setting up and running the plate-motion inversion program. Chuck DeMets and Don Argus provided helpful comments on an early version of this manuscript. We thank Dan McKenzie and an anonymous referee for thoughtful reviews that helped us to improve the manuscript. J.K.M. and R.G.G.'s efforts were supported by NSF grants OCE-0453219, OCE-0928961, and OCE-1131638. The data analyzed herein are taken from *DeMets et al*. [2010] and sources cited therein.

References

Argus, D. F., and R. G. Gordon (1996), Tests of the rigid-plate hypothesis and bounds on intraplate deformation using geodetic data from very long baseline interferometry, *J. Geophys. Res.*, *101*, 13,555–13,572.

Argus, D. F., R. G. Gordon, M. B. Heflin, C. Ma, R. J. Eanes, P. Willis, W. R. Peltier, and S. E. Owen (2010), The angular velocities of the plates and the velocity of Earth's centre from space geodesy, *Geophys. J. Int.*, *180*, 913–960.

Bergman, E. A., J. L. Nábělek, and S. C. Solomon (1984), An extensive region of off-ridge normal-faulting earthquakes in the southern Indian Ocean, *J. Geophys. Res.*, *89*, 2425–2443, doi:10.1029/JB089iB04p02425.

Cochran, J. R. (1979), Analysis of isostasy in the world's oceans: 2. Mid-ocean ridge crests, *J. Geophys. Res.*, *84*, 4713–4729, doi:10.1029/JB084iB09p04713.

Collette, B. J. (1974), Thermal contraction joints in a spreading seafloor as origin of fracture zones, *Nature*, *251*(5473), 299–300, doi:10.1038/251299a0.

Davies, R., P. England, B. Parsons, H. Billiris, D. Paradissis, and G. Veis (1997), Geodetic strain rate of Greece in the interval 1892–1992, *J. Geophys. Res.*, *102*, 24,571–24,588, doi:10.1029/97JB01644.

DeMets, C., and D. S. Wilson (2008), Toward a minimum change model for recent plate motions: Calibrating seafloor spreading rates for outward displacement, *Geophys. J. Int.*, *174*, 825–841, doi:10.1111/j.1365-246X.2008.03836.x.

DeMets, C., R. G. Gordon, D. F. Argus, and S. Stein (1990), Current plate motions, *Geophys. J Int.*, *101*, 425–478, doi:10.1111/j.1365-246X.1990.tb06579.x.

DeMets, C., R. G. Gordon, and P. Vogt (1994), Location of the Africa-Australia-India triple junction and motion between the Australian and Indian plates: Results from an aeromagnetic investigation of the Central Indian and Carlsberg ridges, *Geophys. J. Int.*, *119*, 893–930, doi:10.1111/j.1365-246X.1994.tb04025.x.

DeMets, C., R. G. Gordon, and J.-Y. Royer (2005), Motion between the Indian, Capricorn and Somalian plates since 20 Ma: Implications for the timing and magnitude of distributed lithospheric deformation in the equatorial Indian ocean, *Geophys. J. Int.*, *161*, 445–468.

DeMets, C., R. G. Gordon, and D. F. Argus (2010), Geologically current plate motions, *Geophys. J. Int.*, *181*, 1–80, doi:10.1111/j.1365-246X.2009.04491.x.

Dixon, T. H., A. Mao, and S. Stein (1996), How rigid is the stable interior of the North American plate?, *Geophys. Res. Lett.*, *23*, 3035–3038, doi:10.1029/96GL02820.

England, P., and P. Molnar (1997), Active deformation in Asia: From kinematics to dynamics, *Science*, *278*, 647–650.

Fontaine, F. J., M. Cannat, and J. Escartin (2008), Hydrothermal circulation at slow-spreading mid-ocean ridges: The role of along-axis variations in axial lithospheric thickness, *Geology*, *36*, 759–762.

Gallo, D. G., P. J. Fox, and K. C. Macdonald (1986), A Seabeam investigation of the Clipperton transform fault: The morphotectonic expression of a fast slipping transform boundary, *J. Geophys. Res.*, *91*, 3455–3467, doi:10.1029/JB091iB03p03455.

Gordon, R. G. (1998), The plate tectonic approximation: Plate nonrigidity, diffuse plate boundaries, and global plate reconstructions, *Annu. Rev. Earth Planet. Sci.*, *26*, 615–642.

Gordon, R. G. (2000), Diffuse oceanic plate boundaries: Strain rates, vertically averaged rheology, and comparisons with narrow plate boundaries and stable plate interiors, in *The History and Dynamics of Global Plate Motions*, *Geophysical Monograph*, vol. 121, edited by M. A. Richards, R. G. Gordon, and R. Van der Hilst, pp. 143–159, AGU, Washington, D. C.

Haxby, W. F., and E. M. Parmentier (1988), Thermal contraction and the state of stress in the oceanic lithosphere, *J. Geophys. Res.*, *93*, 6419–6429, doi:10.1029/JB093iB06p06419.
Hillier, J. K., and A. B. Watts (2005), Relationship between depth and age in the north Pacific Ocean, *J. Geophys. Res.*, *110*, B02405, doi:10.1029/2004JB003406.
Horner-Johnson, B. C., and R. G. Gordon (2010), True polar wander since 32 Ma B.P.: A paleomagnetic investigation of the skewness of magnetic anomaly 12r on the Pacific plate, *J. Geophys. Res.*, *115*, B09101, doi:10.1029/2009JB006862.
Huang, J., F. Niu, R. G. Gordon, and C. Cui (2015), Accurate focal depth determination of oceanic earthquakes using water-column reverberation and some implications for the shrinking plate hypothesis, *Earth Planet. Sci. Lett.*, *432*, 133–141, doi:10.1016/j.epsl.2015.10.001.
Kohlstedt, D., L. B. Evans, and S. J. Mackwell (1995), Strength of the lithosphere: Constraints imposed by laboratory experiments, *J. Geophys. Res.*, *100*, 17,587–17,602, doi:10.1029/95JB01460.
Korenaga, J. (2007), Thermal cracking and the deep hydration of oceanic lithosphere: A key to the generation of plate tectonics?, *J. Geophys. Res.*, *112*, B05408, doi:10.1029/2006JB004502.
Kreemer, C., and R. G. Gordon (2014), Pacific plate deformation from horizontal thermal contraction, *Geology*, *42*, 847–850, doi:10.1130/G35874.1.
Kumar, R. R., and R. G. Gordon (2009), Horizontal thermal contraction of oceanic lithosphere: The ultimate limit to the rigid plate approximation, *J. Geophys. Res.*, *114*, B01403, doi:10.1029/2007JB005473.
Luttrell, K., and D. Sandwell (2012), Constraints on 3-D stress in the crust from support of mid-ocean ridge topography, *J. Geophys. Res.*, *117*, B04402, doi:10.1029/2011JB008765.
McKenzie, D. P. (1967), Some remarks on heat flow and gravity, *J. Geophys. Res.*, *72*, 6261–6273, doi:10.1029/JZ072i024p06261.
McKenzie, D. P. (1972), Plate tectonics, in *The Nature of the Solid Earth*, edited by E. Robertson, pp. 323–360, McGraw-Hill, New York.
Parmentier, E. M., and W. F. Haxby (1986), Thermal stresses in the oceanic lithosphere: Evidence from geoid anomalies at fracture zones, *J. Geophys. Res.*, *91*, 7193–7204, doi:10.1029/JB091iB07p07193.
Parson, L. M., P. Patriat, R. C. Searle, and A. R. Briais (1993), Segmentation of the Central Indian Ridge between 12°12′S and the Indian-Ocean Triple Junction, *Mar. Geophys. Res.*, *15*(4), 265–282, doi:10.1007/bf01982385.
Parsons, B., and J. G. Sclater (1977), An analysis of the variation of ocean floor bathymetry and heat flow with age, *J. Geophys. Res.*, *82*, 803–827, doi:10.1029/JB082i005p00803.
Pockalny, R. A., R. S. Detrick, and P. J. Fox (1988), The morphology and tectonics of the Kane transform from sea beam bathymetry data, *J. Geophys. Res.*, *94*, 3179–3194, doi:10.1029/JB093iB04p03179.
Roest, W. R., R. C. Searle, and B. J. Collette (1984), Fanning of fracture zones and a three-dimensional model of the Mid-Atlantic Ridge, *Nature*, *308*, 527–531.
Royer, J.-Y., R. G. Gordon, C. DeMets, and P. R. Vogt (1997), New limits on the motion between India and Australia since chron 5 (11 Ma) and implications for lithospheric deformation in the equatorial Indian Ocean, *Geophys. J. Int.*, *129*, 41–74.
Ryan, W. B. F., et al. (2009), Global multi-resolution topography synthesis, *Geochem. Geophys. Geosyst.*, *10*, Q03014, doi:10.1029/2008GC002332.
Sandwell, D. T. (1986), Thermal stress and the spacings of transform faults, *J. Geophys. Res.*, *91*, 6405–6417, doi:10.1029/JB091iB06p06405.
Sandwell, D., and Y. Fialko (2004), Warping and cracking of the Pacific plate by thermal contraction, *J. Geophys. Res.*, *109*, B10411, doi:10.1029/2004JB003091.
Smith, W. H. F., and D. Sandwell (1997), Global seafloor topography from satellite altimetry and ship depth soundings, *Science*, *277*, 1956–1962, doi:10.1126/science.277.5334.1956.
Turcotte, D. L., and E. R. Oxburgh (1967), Finite amplitude convective cells and continental drift, *J. Fluid Mech.*, *28*, 29–42, doi:10.1017/S0022112067001880.
Turcotte, D. L., and E. R. Oxburgh (1969), Convection in a mantle with variable physical properties, *J. Geophys. Res.*, *74*, 1458–1474, doi:10.1029/JB074i006p01458.
Turcotte, D. L., and E. R. Oxburgh (1973), Mid-plate tectonics, *Nature*, *244*, 337–339.
Wessel, P. (1992), Thermal stresses and the bimodal distribution of elastic thickness estimates of the oceanic lithosphere, *J. Geophys. Res.*, *97*, 14,177–14,193, doi:10.1029/92JB01224.
Wessel, P., and W. F. Haxby (1990), Thermal stresses, differential subsidence, and flexure at oceanic fracture zones, *J. Geophys. Res.*, *95*, 375–391, doi:10.1029/JB095iB01p00375.
Wiens, D. A., and S. Stein (1983), Age dependence of oceanic intraplate seismicity and implications for lithospheric evolution, *J. Geophys. Res.*, *88*, 6455–6468, doi:10.1029/JB088iB08p06455.
Wiens, D. A., and S. Stein (1984), Intraplate seismicity and stresses in young oceanic lithosphere, *J. Geophys. Res.*, *89*, 11,442–11,464, doi:10.1029/JB089iB13p11442.
Wilcock, W. S. D., G. M. Purdy, and S. C. Solomon (1990), Microearthquake evidence for extension across the Kane transform fault, *J. Geophys. Res.*, *95*, 15,439–15,462, doi:10.1029/JB095iB10p15439.
Wilson, J. T. (1965), Transform faults, oceanic ridges and magnetic anomalies southwest of Vancouver Island, *Science*, *150*, doi:10.1126/science.150.3695.482.